Dual-gate Ion-Sensitive Ferroelectric Field-Effect Transistor with Ultra-High Sensitivity >1000 mV/pH and Low Operation Voltage <3 V

Zikang Yao[1,2], Danyang Chen[1,2], Mengwei Si[1], Longchun Wang[1], Xiaojun Guo[1], Jingquan Liu[1*], Wei Tang[2,*] and Xiuyan Li[1,*]
[1] National Key Laboratory of Advanced Micro and Nano Manufacture Technology, Shanghai Jiao Tong University, Shanghai, 200240, China
[2] School of Integrated Circuits (School of Information Science and Electronic Engineering), Shanghai Jiao Tong University, Shanghai, 200240, China
email: jqliu@sjtu.edu.cn, terry_tang@sjtu.edu.cn, xiuyanli@sjtu.edu.cn

2025 IEEE International Electron Devices Meeting (IEDM) | 979-8-3315-6785-9/25/$31.00 ©2025 IEEE | DOI: 10.1109/IEDM50572.2025.11353521

***Abstract*—**This work, for the first time, demonstrates high performance of dual-gate ion-sensitive ferroelectric field-effect transistor (DG-ISFeFET) with antiferroelectric (AFE) $Hf_xZr_{1-x}O_2$ (HZO) film and In_2O_3 (InO) semiconductor. Super-Nernstian sensitivity of >1000 mV/pH is achieved for pH sensing with a low operation voltage of ~3 V, which benefits from current amplification induced by polarization switching in AFE HZO in addition to dual-gate structure optimization. This work paves a novel way to ultra-high ISFET by leveraging CMOS compatible ferroelectric technology.

I. Introduction

Highly-sensitive ion-sensitive field-effect transistors (ISFETs) based pH sensing is crucial in biological/medical diagnostics, environmental monitoring, and industrial process control, where sample volumes are tiny and pH changes subtle [1-3]. Enhanced sensitivity allows earlier detection of abnormalities and more accurate real-time measurements. However, there is a theoretical Nernst limit in sensitivity (~59 mV/pH at 25°C) in ISFETs [4]. In recent years, the Nernst limit has been surpassed via strategy of dual-gate ISFET structure with >500mV/pH sensitivity demonstrated [5-10]. However, such devices are generally with > 150 nm ultra-thick dielectric layer, which require a high operation voltage >15 V. Development of new strategy to achieve scaled devices with high pH sensitivity and low operation voltage is still required.

In this study, by incorporating highly pH-sensitive Al_2O_3 (AlO) layer and high mobility InO channel for DG-ISFET fabrication, we achieve >260 mV/pH sensitivity with a relatively low operation voltage of 3 V. Moreover, through employing AFE $Hf_xZr_{1-x}O_2$ (HZO) film in such a device, we demonstrate a DG ferroelectric ISFET (ISFeFET) with enhanced pH sensitivity >1000 mV/pH at a low operation voltage for the first time, providing a novel way to realize CMOS-based ultra-high sensitivity for pH sensing.

II. Devices Structure and Fabrication

Fig.1 and **Fig.2** shows the structure and fabrication process flow of DG-ISFETs and DG-ISFeFETs. The fabrication began with sputtering 30 nm tungsten (W) as the floating gate on the SiO_2/Si substrate. HZO (Hf:Zr=1:1) film was then grown by atomic layer deposition (ALD) at 250°C, followed by sputtering and patterning 30 nm W to form bottom gate. Then, 4~6 nm InO was deposited by ALD and patterned via HCl etching. After that, 50 nm Ni is formed by thermal evaporation as source/drain (S/D) electrodes, defining 40×60 μm^2 channel area. Subsequent steps included deposition of top gate dielectric AlO by ALD at 100°C which is also used as pH-sensing layer (intrinsic sensitivity of ~45 mV/pH), sputtering of 30 nm W as probe contact area and annealing at 250°C for 30min in air to adjust the threshold voltage (V_{th}). Finally, SU-8 epoxy encapsulation is coated to isolate the other area from solution to prevent parasitic capacitance and leakage current, with AlO corresponding to the channel region exposed only. For DG-ISFeFET, rapid thermal annealing for 30s at 450 ℃ in N_2 ambient was carried out to crystallize the HZO before InO deposition. In addition to device with ferroelectric (FE) HZO (Hf:Zr=1:1), that with AFE HZO (Hf:Zr=1:4) was also prepared by the same steps.

Fig. 3 exhibits optical microscopy images of the fabricated devices with structural details on top view and **Fig. 4** shows cross-section image and element mapping of the devices obtained from transmission electron microscope (TEM). The pH sensing circuit is schematically shown in **Fig. 5**. The reference voltage (V_{ref}) was supplied through the Ag/AgCl reference electrode. The top capacitance (C_{top}) consists of AlO capacitance (C_{AlO}) in series with the electrical double layer (EDL, C_{EDL} for capacitance), while the bottom capacitance (C_{bottom}) comprises metal-oxide-semiconductor (MOS) capacitance (C_{MOS}) in series with a metal-HZO-metal (MHM) capacitance (C_{MHM}). The transfer characteristics (I_{DS}-V_{GS}) measured under a solution of pH=7 with 0.2V step increments of V_{ref} are presented in **Fig. 6**, demonstrating the stable and effective potential control on the channel.

III. High Sensitivity of DG-ISFET

The effect of InO thickness (t_{InO}) on pH sensitivity of DG-ISFET is firstly investigated. **Fig. 7** shows sensing characteristics of InO-ISFET under various pH solutions, with t_{InO} varying from 4 to 6 nm, AlO fixed with 4.4 nm and HZO with 20 nm. The sensitivity is extracted by linearly fitting the voltage change in subthreshold region, corresponding to a current of 10 nA as shown in **Fig.8**. Interestingly, the sensitivity exhibits an enhancement (15.4% higher) with increasing t_{InO} from 4 to 5 nm while it shows negligible gain (3.2% higher) when InO is thicker than 5 nm. The observed sensitivity-thickness relationship is understandable from viewpoint of charge screening effects. When channel is relatively thin, increased thickness provide more carriers for effective surface screening, enhancing sensitivity. However,

when InO becomes relatively thick, the channel already contains sufficient carriers to fully screen interfacial potential changes, making sensitivity enhancement saturated. Notably, thicker InO causes negative shift of V_{th} and hence larger operation voltage indicated in **Fig. 8(d)**, so 5 nm InO is used in the following part.

Then the top-bottom capacitive coupling effect on the sensitivity is considered. It has been well agreed that the capacitance ratio of top and bottom gate (C_{top}/C_{bottom}) is critical to break through the Nernst limit in DG-ISFET, characterized as $dV_{th}/dpH \propto C_{top}/C_{bottom}$ [11]. Therefore, to achieve an enhanced sensitivity, the thickness of both AlO (t_{AlO}) and HZO (t_{HZO}) layers of above devices was further engineered. **Fig. 9** shows the t_{AlO} dependence of pH sensitivity of DG-ISFET with 10 nm HZO. The device with 5 nm AlO demonstrates about twice sensitivity of that with 10 nm one, attributed to its approximately doubled C_{top} and consistent with expectation from C_{top}/C_{bottom} effect. However, the thinner AlO would cause permeation of pH solution through AlO into channel, degrading the performance of the devices. Similarly, 20/15 nm HZO enables about 2/1.5 times higher sensitivity than 10 nm one due to 2/1.5 times lower C_{bottom} as summarized in **Fig. 10.** As a result, a sensitivity of 264 mV/pH is obtained from the device with 4.4 nm AlO and 20 nm HZO within an operating voltage of 3 V. But note that thicker HZO film also naturally causes subthreshold swing (SS) degradation and negative shift of V_{th}, resulting in undesired increase of operation voltage. Therefore, 10 nm HZO is used in the following part as a balanced designing. Moreover, based on above results, the sensitivity gain would be further enhanced by increasing C_{top}/C_{bottom} via engineering area ratio of bottom gate to channel (AR) as expected in **Fig. 11,** where a reference sample with 5 nm AlO and 10 nm HZO is considered.

IV. Ultra-high sensitivity of DG-ISFeFET

We next change HZO to be with high performance of FE and AFE properties by crystallizing HZO films and adjusting Hf:Zr ratio. The polarization-voltage (P-V) measurement of FE and AFE capacitors are shown in **Fig. 12. Fig. 13** shows the FeFET I_{DS}-V_{GS} curves with FE and AFE layers, obtaining a counterclockwise hysteresis induced by polarization switching under electric field. Generally, wider hysteresis indicates better FeFET performance, so AFE HZO provides better performance than FE one. This has been explained in our previous work [12]. Note that engineering of the AR to divide sufficient potential on HZO is also important for getting high performance of FeFETs and AR=1:4 is obtained as the optimized designing. In addition, dielectric constant (κ) of FE and AFE HZO is much enhanced compared with that of amorphous one as shown in **Fig. 14**. Concerning both changes in κ and AR, C_{top}/C_{bottom} of devices with FE and AFE are 2.38 and 1.8 times higher than that of the reference sample in **Fig.11**, respectively.

Fig. 15 and **Fig. 16** show the pH sensing characteristics of DG-ISFeFETs with FE and AFE HZO. The I_{DS}-V_{GS} curves of DG-ISFeFET with FE HZO is degraded greatly while that with AFE HZO looks much better**.** Interestingly, the device with AFE HZO shows an enhanced pH sensitivity (>1000 mV/pH) in the forward scanning of V_{GS} while suppressed one (<130 mV/pH) in the backward under an operation voltage within 3 V as summarized in **Fig. 17**. Namely, an over 3 times extra gain in pH sensitivity is obtained in forward scanning from this device compared to predicted result from DG-ISFET with paraelectric HZO as suggested in **Fig.18**. The performance of the device with AFE HZO is further confirmed by current-time measurement (I-T) under various pH solutions as shown in **Fig. 19**, suggesting the sensing performance can be reliably obtained under static measurements as well. These results indicate that the polarization switching direction in AFE layer has a tuning effect on pH sensing.

We next understand the physics of the tuning effect of polarization switching in AFE HZO layer on pH sensitivity of DG-ISFeFET. Protons (H^+, positively charged) adsorb onto the Al_2O_3/electrolyte interface, inducing negative charges on the floating gate via electrostatic coupling. During forward scanning of V_{GS}, the polarization in AFE HZO layer switched from down to up direction, injecting additional negative charges into the floating gate, which enhances channel carrier density and results in current increase. Conversely, during backward scanning, reversed polarization switching occurs, injecting compensatory positive charges that suppress channel conductivity. The high performance of FeFET with a large counterclockwise hysteresis is significant to get this effect due to distinct polarization switching in forward and backward scanning. These views are schematically shown in **Fig. 20.**

Finally, **Table. I** compares the sensitivity and operation voltage of our strategy with those reported in literatures [5-10]. For an ultra-high sensitivity >1000 mV/pH, we achieved record low operation voltage of 3V based on a completely new physics of DG-ISFeFET, which is 5 times lower than the lowest value obtained from common DG-ISFET reported previously.

V. Conclusion

This work demonstrated a new kind of DG-ISFeFET with AFE HZO layer, showing more than 3 times extra enhancement in sensitivity compared with the same structure of DG-ISFET. The physics of extra enhancement in sensitivity is understood from channel current amplification induced by polarization switching from down to up in AFE HZO. And based on this, an ultra-high pH sensitivity >1000 mV/pH is achieved under the record low operation voltage of 3 V.

Acknowledgment

This work is supported National Natural Science Foundation of China (62274109, 6245003, 62474106) and Shanghai Pilot Program for Basic Research - Shanghai Jiao Tong University (21TQ1400212)

References

[1]Q. Liu et al., iScience, 2020.[2]G. K. Saba et al., Front. Mar. Sci., 2019. [3]J. M. Margarit-Taulé et al., Sens. Actuators B, 2022.[4]P. Bergveld, Sens. Actuators B, 2003. [5]E.-K. Hong and W.-J. Cho, Sens. Actuators B., 2021. [6]D. Bhatt et al, ACS Appl. Electron. Mater., 2020. [7]J.-H. Jeon et al, Sci. Technol. Adv. Mater., 2020. [8]D. Bhatt and S. Panda, ACS Appl. Electron. Mater.,2021. [9]C.-H. Lu et al, IEEE TED., 2018. [10]K. Takechi et al., JJAP., 2015. [11]M. Spijkman et al., AFM., 2010. [12]T. Cui et al., IEEE EDL., 2024.

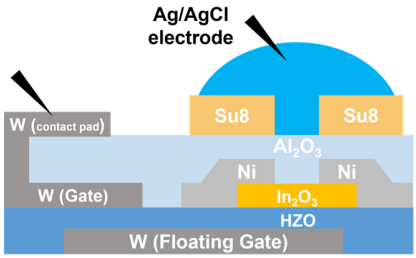

Fig.1 Schematic of the DG-ISFET biosensor with Ag/AgCl reference electrode featuring an AlO/EDL top stack and a W/HZO/W/HZO/InO bottom stack.

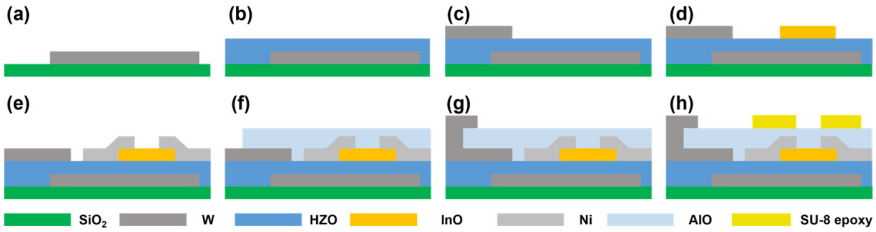

Fig. 2 Fabrication process flow of DG-ISFET including:**(a)** floating gate deposition, **(b)** HZO grown by ALD, **(c)** gate (bottom) deposition, **(d)** channel patterning, **(e)** S/D evaporation, **(f)** AlO grown by ALD, **(g)** deposition of probe contact pads, **(h)** SU-8 encapsulation.

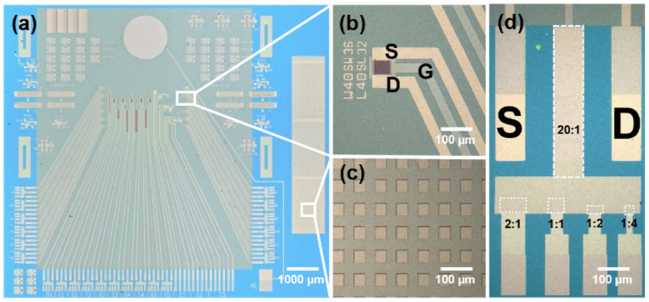

Fig. 3 Microscopy images of **(a)** top view of the full 1.8×1.8 cm^2 device, **(b)** the 40×60 μm^2 channel area, **(c)** 40×40 μm^2 isolated MHM capacitors and **(d)** gate electrodes with various AR from 20:1 to 1:4.

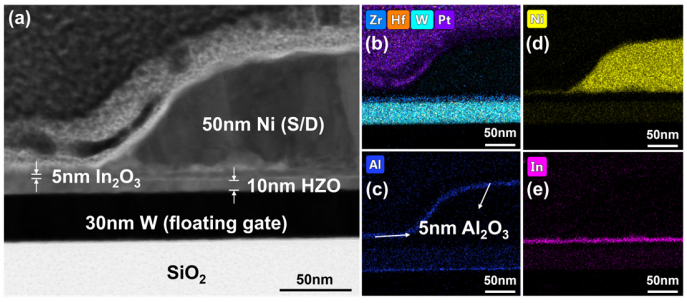

Fig. 4 TEM image of **(a)** the cross-section of the channel region and corresponding energy-dispersive X-ray spectroscopy (EDS) mapping of **(b)** Zr, Hf, W, Pt, **(c)** Al, **(d)** Ni, and **(e)** In elements.

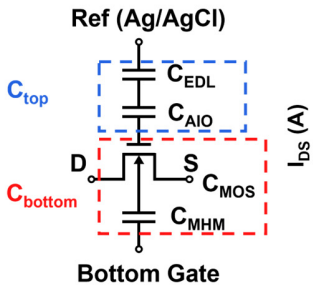

Fig. 5. Macromodel for DG-ISFET, where C_{top} and C_{bottom} are capacitances for C_{EDL}/C_{AlO} and C_{MOS}/C_{MHM} in series, respectively.

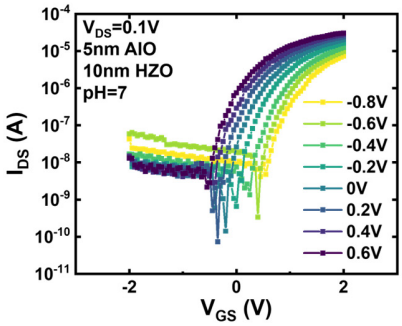

Fig. 6 I_{DS}-V_{GS} curves of the DG-ISFET under varying V_{ref} from -0.8V to 0.6V in pH7 solution with 0.2V of step increments.

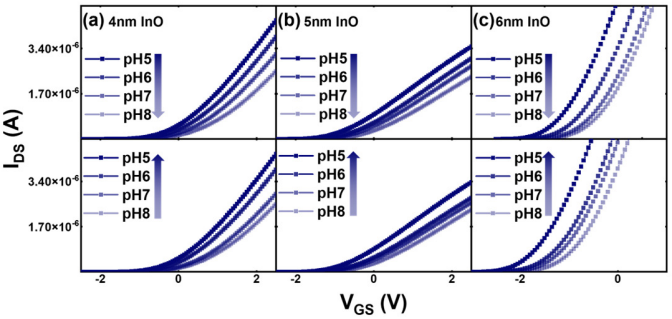

Fig. 7 pH-dependent I_{DS}-V_{GS} curves of DG-ISFETs with 4.4 nm AlO, 20 nm HZO and varying t_{InO}. **(a)** 4 nm, **(b)** 5 nm, and **(c)** 6 nm InO devices exhibit systematic V_{th} shifts with pH variation (pH5-8-5) corresponding to the current of 10 nA.

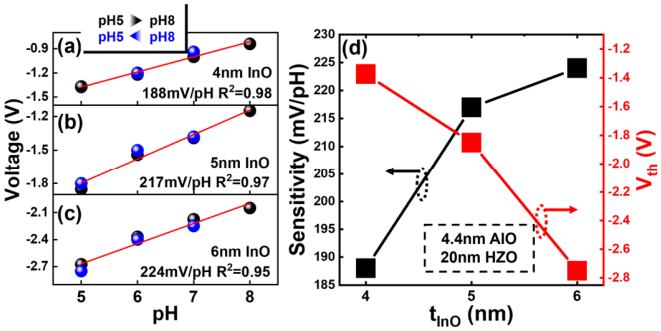

Fig. 8 Extracted sensitivity by linearly fitting with pH variation (pH5-8-5) under various t_{InO} of **(a)** 4 nm, **(b)** 5nm and **(c)** 6nm and **(d)** its relationship between sensitivity and V_{th}.

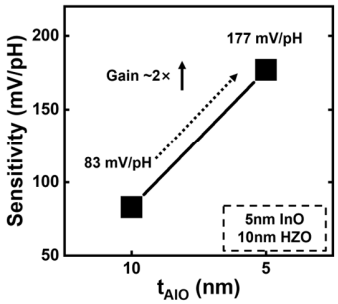

Fig. 9 Impact of t_{AlO} on sensitivity in DG-ISFETs with 10 nm and 20 nm HZO bottom gate dielectrics.

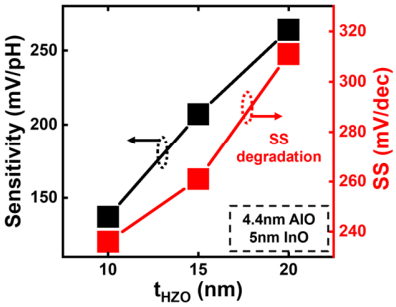

Fig. 10 Impact of HZO thickness (t_{HZO}) on sensitivity and SS with 4.4 nm AlO top gate dielectric.

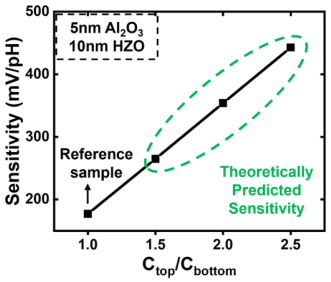

Fig. 11 AR-dependent capacitance and predicted sensitivity trend of the DG-ISFET.

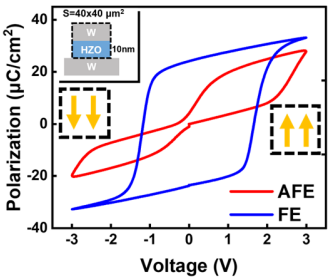

Fig. 12 P-V hysteresis characteristics of 10 nm HZO-based FE and AFE capacitor with 40×40 μm² area.

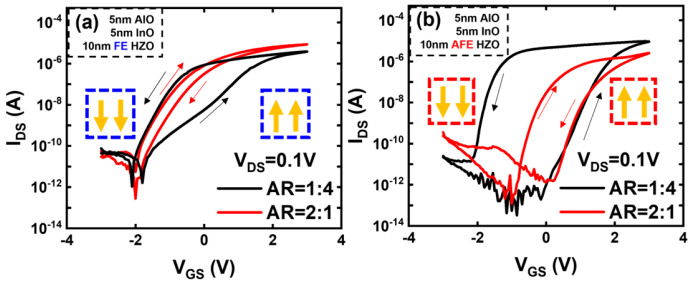

Fig. 13 I_{DS}-V_{GS} curves of FeFETs with **(a)** FE HZO and **(b)** AFE HZO in air under AR=2:1 and 1:4. Smaller capacitance (AR=1:4) allocates more voltage on MHM capacitors, inducing a counterclockwise hysteresis.

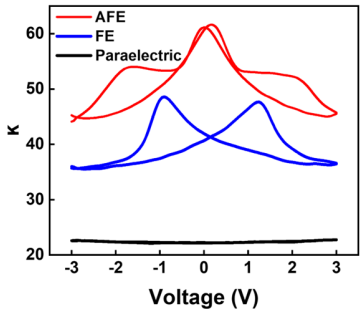

Fig. 14 κ extracted from MHM capacitors by C-V measurement for FE, AFE and paraelectric HZO with AR=1:4.

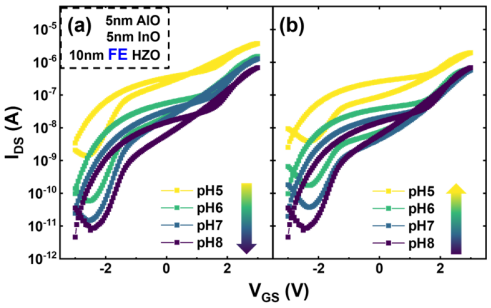

Fig. 15 pH-dependent I_{DS}-V_{GS} curves of device with 5 nm AlO and 10 nm FE HZO under pH variation of **(a)** pH 5-8 and **(b)** pH 8-5.

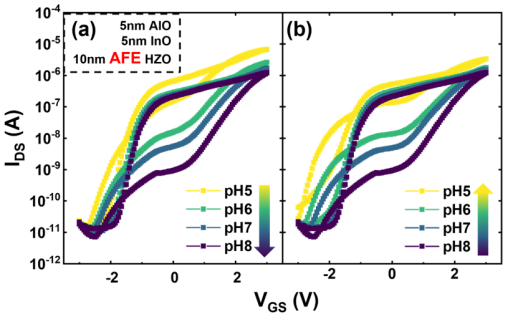

Fig. 16 pH-dependent I_{DS}-V_{GS} curves of device with 5 nm AlO and 10 nm AFE HZO under pH variation of **(a)** pH 5-8 and **(b)** pH 8-5.

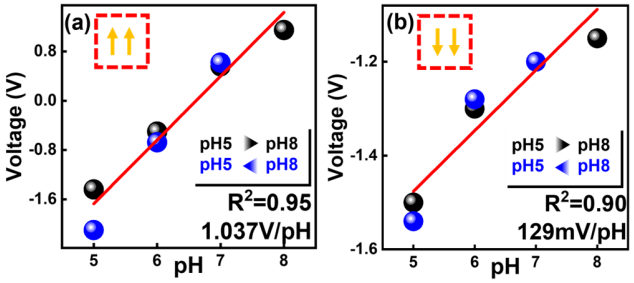

Fig. 17 Extracted sensitivity of 10 nm AFE HZO devices under V_{GS} **(a)** increase from -3 to 3V and **(b)** decrease from 3 to -3V with pH variation (pH5-8-5) corresponding to the current of 10 nA.

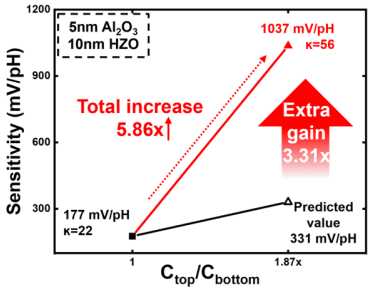

Fig. 18 Comparison of DG-ISFET and DG-ISFeFET in terms of κ and sensitivity, with a 3.31× extra sensitivity enhancement.

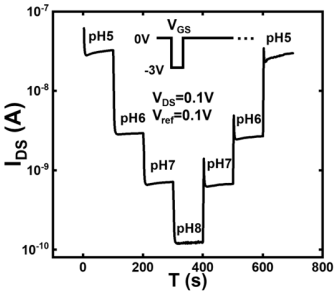

Fig. 19 I-T curve of DG-ISFeFET with AFE HZO with **(a)** applied V_{GS} and **(b)** corresponding pH response.

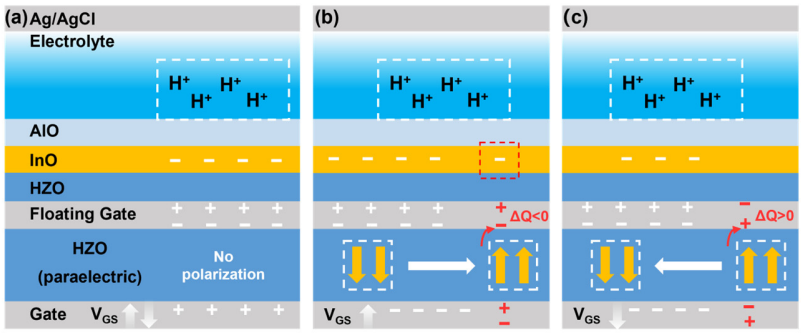

Fig. 20 Physics for extra sensitivity enhancement. **(a)** In paraelectric sample, floating gate charges depend solely on H^+ concentration without polarization effects, showing identical sensitivity for forward/backward V_{GS} sweeps. For AFE-HZO one, **(b)** in forward sweep: negative charges injection from polarization switching enhances sensitivity and **(c)** in reverse sweep, opposite polarization transition injects positive charges, suppressing pH response.

Sensor	Sensitivity (mV/pH)	Thickness of Gate stack	Operation Voltage (V)	Ref
DG-ISFET	998	300nm SiO_2	<32	[5]
DG-ISFET	847	150nm SiO_2	<30	[6]
DG-ISFET	2364	200nm SiO_2	<30	[7]
DG-ISFET	917	150nm SiO_2	<20	[8]
DG-ISFET	937	200nm SiO_2	<25	[9]
DG-ISFET	450	200nm SiO_2	<15	[10]
DG-ISFeFET	1037	10nm HZO	<3	This work

Table. I Comparison of pH sensing performance from devices in this work with those reported, demonstrating this work's breakthrough in simultaneously achieving super Nernst limit sensitivity, sub-3V low operation voltage, and thin gate stack.